

Design of Nanosensors for Fissile Materials in Nuclear Waste Water

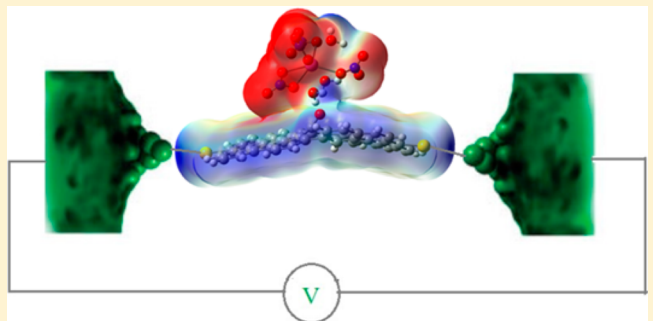
Narendra Kumar[†] and Jorge M. Seminario*,^{†,‡,§}

[†]Department of Chemical Engineering, Texas A&M University, 3122 TAMU Room 200, College Station, Texas 77843, United States

[‡]Department of Materials Science and Engineering, Texas A&M University, 503 Mechanical Engineering Office Building (MEOB), College Station, Texas 77843, United States

[§]Department of Electrical and Computer Engineering, Texas A&M University, 3128 TAMU, College Station, Texas 77843, United States

ABSTRACT: Uranium and plutonium ions and their complexes play an important role in nuclear fuel reprocessing, and their trace characterization is important in nuclear forensics. In this work, we perform ab initio density functional theory calculations of U and Pu complexes with graphene and graphene oxide to examine the applicability of a graphene-based fissile sensor. We find that graphene needs to be functionalized to act as an effective sensor for detection of fissile materials such as uranium and plutonium complexes. This is because characteristic changes in the plasmonic properties of a finite graphene sheet, molecular electrostatic potentials, and current–voltage characteristics in oxidized graphene nanojunctions are strong signatures of the sorption of uranium or plutonium moieties.



INTRODUCTION

Uranium and plutonium oxides and their complexes are major constituents present in soils and groundwater around contaminated sites as well as near production facilities.^{1–3} Dissolved uranium is predominantly present in the form of uranyl(VI) complexes.¹ Plutonium is known to exist in aqueous solution in four different oxidation states, III, IV, V, and VI, with the last two as the dioxo-species PuO_2^+ and PuO_2^{2+} .⁴ Molecular dynamics simulations have been used to study the structure and hydration of uranyl ions and their several complexes in water,^{1,5–8} although similar studies for plutonyl ions and their complexes are lacking. The uranyl ion in aqueous phase was reported to form pentagonal bipyramidal structure with five water molecules lying in equatorial plane. In the presence of counterions (CO_3^{2-} , OH^- , and NO_3^-), one or two water molecules in the first shell are replaced by the counterions preserving five-fold symmetry. Unlike uranyl ions, U^{3+} , Pu^{3+} , and Pu^{4+} form 9–10 coordination with water molecules.^{9,10} There is a strong electron transfer observed, and counterions are strongly bonded to the central actinide ion.

The contamination of groundwater due to accidental leakage of radioactive wastes poses a grave danger to the environment and human life, and hence trace characterization of these radioactive materials is essential in nuclear forensics. The design and fabrication of electronic molecular devices as sensors for plutonium and uranium using theoretical and experimental studies has gained paramount importance in the nuclear community. Recently, it was found that flakes of graphene oxide (GO) added to water caused radionuclides to condense into clumps.¹¹ Experiments were conducted with water containing several actinides including U and Pu along with Ca and Na to

study their interaction with GO. GO is shown to be more effective in removal of radionuclides compared with traditional bentonite clays and activated carbon.¹¹ GO can be prepared by oxidizing a large flake of graphite using potassium permanganate in the presence of sulphuric and phosphoric acids.¹¹ GO is partially oxidized and highly amorphous; due to random arrangement of functional groups and large structural disorder in the carbon skeleton, detailed atomic structure is still elusive. Common functional groups reported on oxidation of graphene are $-\text{COOH}$, $-\text{OH}$, $-\text{C}=\text{O}$ at edges, and $\text{C}-\text{O}-\text{C}$ and $-\text{OH}$ on the basal plane.^{13–16}

The plasmonic features of nanosized graphene sheets (or GOs) are strongly coupled to their electrical, magnetic, vibrational, and optical characteristics and to those of the moieties that may attach to the graphene molecule such as nuclear agents. When these moieties interact with the graphene plasmons, an enhancement (amplification) of observable quantities from the moieties is observed in the whole molecule, as successfully observed in the past with chemical and biological agents.¹² Theoretical simulations have shown the possible use for sensors to identify single molecules with high selectivity and sensitivity that will contribute to the miniaturization as well as efficient transport and processing of signals using graphene-based devices.¹² It is expected that this approach will allow us not only to sense targeted agents but also to perform chemical recognition using molecular electrostatic potentials (MEPs), which have become the signature on the nanoscale, perfectly

Received: August 18, 2013

Revised: October 13, 2013

Published: October 16, 2013

suitable for detection and identification of atoms and small molecules.¹² Changes in the MEP due to the presence of a foreign moiety near graphene or GO can be transduced and amplified into current–voltage characteristics on the nanoscale.¹² By comparing the change in current due to the presence of U or Pu complexes near a graphene and GO, we should be able to detect trace amounts of these radionuclides.

There is abundant literature available on ab initio calculations for uranyl and plutonyl and their several complexes.^{2,17–21} The ground state of the plutonyl ion (PuO_2^{2+}) has been determined as $^3\text{H}_g$, while that of uranyl (UO_2^{2+}) is found to be $^1\Sigma_g^+$.²² The hydration of uranyl and plutonyl has been studied using Kohn–Sham density functional theory (DFT) calculations, in both the gas and aqueous phase.¹⁷ The actinyls were shown to form strong bound complexes with the surrounding water molecules, with pentagonal bipyramidal geometry being the most stable.¹⁷ Ab initio molecular orbital (MO) calculations on the structure and stability of nitrate and sulfate complexes of uranyl and plutonyl have been also reported in literature.² Quantum mechanics calculations were also reported for silicate, phosphate, and arsenate complexes of uranyl to study the bonding characteristics, structure, and spectra of $\text{H}_2\text{UO}_2\text{SiO}_4(\text{H}_2\text{O})_3$, $\text{H}\text{UO}_2\text{PO}_4(\text{H}_2\text{O})_3$, and $\text{HUO}_2\text{AsO}_4(\text{H}_2\text{O})_3$.¹⁸

Other studies include ab initio calculations of equilibrium structure, vibrational frequencies, and bonding characteristics of actinyls, UO_2^{2+} , NpO_2^+ , and PuO_2^{2+} , as well as their hydrated forms, $\text{AnO}_2(\text{H}_2\text{O})_n^{z+}$ ($n = 4, 5, 6$; $z = 1, 2$),¹⁹ where An indicates the actinide group atom. The calculated solvation free energies suggest that five- and six-coordinate complexes are equally preferred for UO_2^{2+} , and five-coordinate species are preferred for NpO_2^+ and PuO_2^{2+} .¹⁹ The electronic and spectroscopic properties of plutonyl carbonate complexes of the type PuO_2CO_3 and the hydrated forms, $\text{PuO}_2\text{CO}_3(\text{H}_2\text{O})_n$ ($n = 1, 2$), have been reported using DFT, Møller–Plesset second-order perturbation theory, and coupled-cluster techniques.²⁰ The structure, vibration spectra, and electron density plots of plutonyl mono-, di-, and tri-carbonate complexes were also reported.²¹ The structural properties of aquo and nitrate complexes of PuO_2^{2+} and Pu^{4+} in addition to the aquo-chloro complexes of PuO_2^{2+} have been extensively studied in both gas and aqueous phases using DFT with scalar relativistic effective core potentials (RECPs) and the polarizable continuum solvation model.²³ The solvation of Pu^{3+} ion in water was investigated using relativistic DFT to determine binding energies and optimized geometries for different coordination numbers of water molecules.³ The DFT study of structure and stability of Pu(III) and Pu(IV) complexes revealed that the maximal number of chloride ions in the first coordination sphere of Pu(III) and Pu(IV) ions is eight and that the extra ninth chloride ion migrated to the second-coordination sphere.²⁴

On the basis of the above and owing to their strong vibronic, plasmonic, and electronic properties, we test in this work the applicability of graphene and GO as sensing molecules for radionuclides such as U and Pu. The next section will describe the Methodology, followed by the Results and Discussion.

METHODOLOGY

We use DFT^{25,26} with the B3PW91, which is a hybrid functional of the Becke exchange²⁷ combined with a Hartree–Fock^{28–30} component and the correlation functional of Perdew–Wang^{31–35}. This functional has been used successfully

in a variety of applications involving related clusters of atoms^{36–39} and other applications involving molecular electronics devices.^{40,41} It has also been used in applications involving metallic clusters.^{42–48} All of the DFT calculations are performed with the program Gaussian 09.⁴⁹ Stuttgart effective core potential and associated basis set are used for plutonium and uranium,^{50,51} and the LANL2DZ basis set and effective core potentials are used for the gold atoms.^{52–54} The ECP parameters for Au have been derived from atomic wave functions obtained in relativistic Hartree–Fock calculations^{52–54} and hence include some relativistic effects, while the ECP parameters for U and Pu are based on a quasi-relativistic level of theory.^{50,51} Successful comparison with experiment for Pu was reported (experimental values inside parentheses) for the ionization potentials 5.69–5.74 eV (6.03 eV)^{50,51} and for the geometry of several plutonium complexes, for example, $\text{PuO}_2(\text{H}_2\text{O})_5^{2+}$: $\text{Pu}–\text{O} = 1.72 \text{ \AA}$ (1.74 Å) and $\text{Pu}–\text{O}_w = 2.44 \text{ \AA}$ (2.41 Å); $\text{PuO}_2(\text{NO}_3)_2(\text{H}_2\text{O})_2$: $\text{Pu}–\text{O} = 1.74 \text{ \AA}$ (1.73 Å), $\text{Pu}–\text{O}_w = 2.53 \text{ \AA}$ (2.43 Å), and $\text{Pu}–\text{O}_N = 2.46 \text{ \AA}$ (2.50 Å); $\text{PuO}_2(\text{Cl})_2(\text{H}_2\text{O})_3$: $\text{Pu}–\text{O} = 1.73 \text{ \AA}$ (1.75 Å), $\text{Pu}–\text{O}_w = 2.53 \text{ \AA}$ (2.49 Å), and $\text{Pu}–\text{Cl} = 2.67 \text{ \AA}$ (2.70 Å); and $\text{Pu}(\text{H}_2\text{O})_8^{4+}$: $\text{Pu}–\text{O}_w = 2.39 \text{ \AA}$ (2.39 Å).²³ Stuttgart ECP, as implemented in Gaussian 09, has also been used to study hydration and oxidation study of plutonyl ion in gas phase.⁶¹ For other atoms present in the system, the 6-31G(d) basis set is used.⁵⁵ The self-consistent approach to find the wave function is performed with a convergence threshold on the density matrix of 10^{-6} and 10^{-8} for the root-mean square and maximum density matrix error between iterations, respectively. Geometry optimizations are carried out with the Berny method.^{56,57} All of the optimized stable structures are checked to be local minima by calculating the Hessian matrix, that is, the second derivative of the energy with respect to all coordinates. When we find that a structure yields negative Hessian eigenvalues, the geometry is modified accordingly to reach a stable structure. The current–voltage curves for the graphene and GO along with other moieties are calculated using the program GENIP developed by our group.^{58–60} The effect of the neighbor contact atoms to the graphene (gold atoms in this case) is directly considered in the discrete ab initio calculations by an extended molecule, which, in addition, is connected to the continuum of states of nanoelectrodes. The GENIP program uses a combination of density functional and Green's functions theories considering the discrete states of the molecular systems and the continuous electronic states of the gold nanocontacts.

RESULTS AND DISCUSSION

Several authors have used Stuttgart small-core scalar RECP to study structure of plutonium complexes and have shown that RECP showed good agreement with experimental results. The structural properties of aquo and nitrate complexes of PuO_2^{2+} and Pu^{4+} in addition to the aquo-chloro complexes of PuO_2^{2+} have been extensively studied in both gas and aqueous phases using DFT with effective core potentials and the polarizable continuum solvation model.²³ The first ionization potential of plutonium using B3PW91/ECP60MWB-SEG is estimated to be 5.72 eV, which is close to the available experimental value of 6.03 eV;⁶² however, it is much closer to the 5.69 to 5.74 eV obtained with the same basis set but with state-averaged CASSCF with subsequent multireference-averaged coupled-pair functional calculations.^{50,51} To confirm that the chosen level of theory correctly identifies lowest energy spin-state, two or more

spin states are considered for each of the bare ions, Pu^{4+} , PuO_2^+ , and PuO_2^{2+} studied here (Table 1). The lowest spin

Table 1. Properties of Several Spin States of Pu^{4+} , PuO_2^{2+} , and PuO_2^{1+} Ions

complex	<i>m</i>	Pu–O	<i>q</i> (Pu)	<i>q</i> (O)	energy
Pu^{4+}	1		4		-551.04015
Pu^{4+}	3		4		-551.14892
Pu^{4+}	5		4		-551.19622
Pu^{4+}	7		4		-550.63525
Pu^{4+}	9		4		-550.07474
PuO_2^{2+}	1	1.654	2.15	-0.08	-703.61595
PuO_2^{2+}	3	1.656	2.15	-0.08	-703.65683
PuO_2^{2+}	5	1.711	2.19	-0.09	-703.63662
PuO_2^{1+}	2	1.690	1.56	-0.28	-704.21144
PuO_2^{1+}	4	1.707	1.59	-0.29	-704.28787
PuO_2^{1+}	6	1.761	1.64	-0.32	-704.20830

state of the Pu^{4+} is found to be quintet, PuO_2^+ quartet, and PuO_2^{2+} triplet. We find the ground state of uranyl to be a singlet using the B3PW91 functional; this result is similar to those reported in previous work.²²

Several multiplicities are also checked for other complexes to confirm that addition of other components does not alter the lowest spin state of bare ion (Table 2). In all cases, it is found that the lowest energy spin state of the complex is the same as that of the corresponding bare ion. It has already been reported that the lowest-energy spin-state for successive hydrates of the bare ions is found to be the same as that of AnO_2^{z+} ($z = 1, 2$), where An indicates U, Np, or Pu.⁶¹

Results from geometry optimization of some common U and Pu complexes present in nuclear wastewater are shown in Figure 1 along with their concentration. All geometries are fully optimized at B3PW91//ECP60MWB-SEG/6-31G(d) level of theory. Local minima are confirmed with the positive eigenvalues of the second derivative of the energy with respect to all coordinates. The bond lengths, energy, and Mulliken charges for several U and Pu complexes are listed in Table 3 and 4.

When these uranyl or plutonyl complexes interact with a graphene molecule (Figure 2), the Pu–O and U–O bond lengths increase, thus indicating weakening of these bonds due to interactions of the actinide ions with graphene. Table 5 lists the bond distances of some U/Pu complexes for comparison purposes.

Molecular Electrostatic Potential. Figure 3 shows the MEPs of U and Pu complexes adsorbed on graphene. The magnitude of the potentials is shown by the solid surface colors. Blue is the most positive potential, and red is the most negative. All complexes are shown on the same color scale (bottom of Figure 3). The electrostatic field is able to modulate the properties of graphene plasmons (sea of π -electrons on the graphene surface), as typically done by the potential in the gate of a field-effect transistor. Graphene electrical and optical responses depend on the interaction of those plasmons with the moieties attached to the graphene surface; we suggest that plasmons are highly sensitive and are likely to be affected by the electrostatic field of a single molecule. Indeed, a significant change in the electrostatic field of graphene was observed when interacting with the Pu and U complexes (Figure 3). A potential challenge for the detection is that some waters are closer to graphene than are Pu or U, indicating the need for graphene functionalization to enhance sensitivity. All calculations have been done at B3PW91 level using Stuttgart ECP for U and Pu and the 6-31G(d) for other atoms.

Interaction of U and Pu Complexes with Graphene Oxide. The interaction of plutonium complex with GO has been studied using two types of structure of GO (Figure 4a,b). As indicated above, when graphene is oxidized to form GO, there is random arrangement of different types of functional groups on the graphene sheet due to partial oxidation. For our study, we have used (i) a GO with two –OH and one –O– functional groups present or type I and (ii) a GO containing a carbonyl functional group or type II. It should be noted that introduction of –CO group on GO leads to breaking of few bonds, and hence those C atoms are saturated with H atoms to satisfy the valence of carbon atoms. The plutonium complex used for this study is plutonium nitrate with few water molecules surrounding it. Nitrates form very strong bonds with Pu(IV) ion, and hence a real comparison can be made with respect to its interaction with GO. As it can be seen in Figure 4a, when plutonium nitrate complex approaches type-I GO, water molecules still remain closest to the GO nanosheet, indicating weak interaction between plutonium ion and GO (type I). This observation is similar to the one found for the interaction of plutonium complex with graphene nanosheet. The MOs also corroborate the fact that –OH and –O– do not cause strong interaction with Pu(IV) complex as HOMO and LUMO of GO (type I) remain unaffected by the presence of Pu(IV) complex. Hence a GO with carbonyl group (type II)

Table 2. Calculated Properties of Several Plutonium Complexes: *q* = Complex Net Charge, *m* = Multiplicity, Pu–O Distance, Pu–O_w Distance, *q*(A) = Partial Charge in Atom A, and Total Energy

complex	<i>q</i>	<i>m</i>	Pu–O	Pu–O _w	<i>q</i> (Pu)	<i>q</i> (O)	<i>q</i> (O _w)	<i>q</i> (H _w)	energy
$\text{PuO}_2^{2+}(\text{H}_2\text{O})_5$	2	1	1.695	2.438	1.59	-0.26	-0.83	0.51	-1085.95722
$\text{PuO}_2^{2+}(\text{H}_2\text{O})_5$	2	3	1.698	2.441	1.59	-0.27	-0.83	0.51	-1085.99667
$\text{PuO}_2(\text{NO}_3)_2(\text{H}_2\text{O})_2$	0	1	1.712	2.520	1.41	-0.33	-0.79	0.47	-1417.77320
$\text{PuO}_2(\text{NO}_3)_2(\text{H}_2\text{O})_2$	0	3	1.716	2.510	1.42	-0.34	-0.80	0.48	-1417.81304
<i>cis</i> - $\text{PuO}_2(\text{Cl})_2(\text{H}_2\text{O})_2$	0	1	1.72	2.492	0.94	-0.34	-0.79	0.49	-1777.69323
<i>cis</i> - $\text{PuO}_2(\text{Cl})_2(\text{H}_2\text{O})_2$	0	3	1.72	2.488	0.96	-0.34	-0.79	0.49	-1777.72976
<i>trans</i> - $\text{PuO}_2(\text{Cl})_2(\text{H}_2\text{O})_2$	0	1	1.72	2.465	1.02	-0.34	-0.79	0.48	-1777.69659
<i>trans</i> - $\text{PuO}_2(\text{Cl})_2(\text{H}_2\text{O})_2$	0	3	1.72	2.464	1.03	-0.34	-0.79	0.48	-1777.73405
<i>cis</i> - $\text{PuO}_2(\text{Cl})_2(\text{H}_2\text{O})_3$	0	1	1.72	2.587	0.95	-0.34	-0.80	0.47	-1854.09703
<i>cis</i> - $\text{PuO}_2(\text{Cl})_2(\text{H}_2\text{O})_3$	0	3	1.72	2.582	0.97	-0.34	-0.80	0.47	-1854.13428
<i>trans</i> - $\text{PuO}_2(\text{Cl})_2(\text{H}_2\text{O})_3$	0	1	1.71	2.523	1.03	-0.33	-0.79	0.47	-1854.10337
<i>trans</i> - $\text{PuO}_2(\text{Cl})_2(\text{H}_2\text{O})_3$	0	3	1.72	2.523	1.04	-0.33	-0.79	0.47	-1854.14221

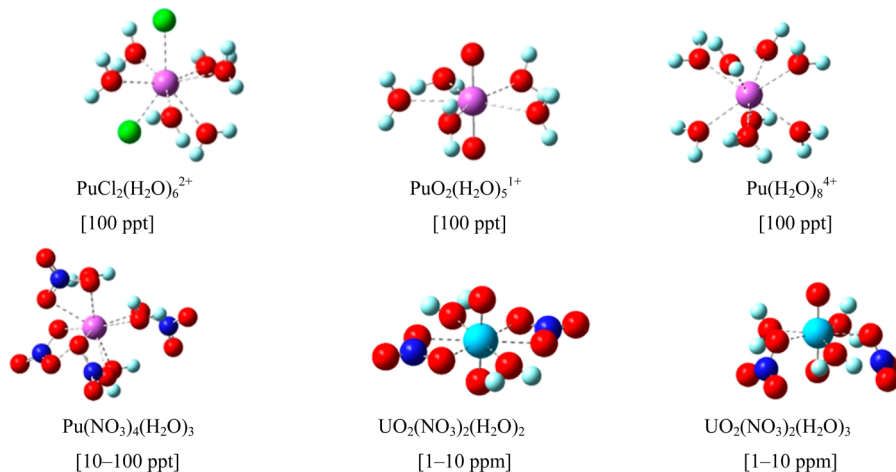


Figure 1. Common U and Pu moieties in nuclear wastewater.

Table 3. Calculated Bond Distance, Atomic Mulliken Charges, and Energies of AnO_2^{z+} ($z = 1, 2$; An = U, Pu) Complexes

complex	q	m	An–O	An–O _w	$q(\text{An})$	$q(\text{O})$	$q(\text{O}_w)$	$q(\text{H}_w)$	energy
PuO_2^{2+}	2	3	1.656		2.15	-0.08			-703.65683
$\text{PuO}_2(\text{H}_2\text{O})_2^{2+}$	2	3	1.696	2.373	1.66	-0.25	-0.83	0.52	-1009.57653
$\text{PuO}_2(\text{H}_2\text{O})_5^{2+}$	2	3	1.698	2.441	1.59	-0.27	-0.83	0.51	-1085.99667
$\text{PuO}_2(\text{H}_2\text{O})_6^{2+}$	2	3	1.701	2.432 ^a	1.56	-0.28	-0.83	0.51	-1162.42399
$\text{PuO}_2(\text{NO}_3)_2(\text{H}_2\text{O})_2$	0	3	1.716	2.510	1.42	-0.34	-0.80	0.48	-1417.81304
PuO_2^{1+}	1	4	1.707		1.59	-0.29			-704.28787
$\text{PuO}_2(\text{H}_2\text{O})^{1+}$	1	4	1.719	2.403	1.48	-0.33	-0.83	0.51	-780.73266
$\text{PuO}_2(\text{H}_2\text{O})_2^{1+}$	1	4	1.731	2.452	1.41	-0.36	-0.83	0.50	-857.16925
$\text{PuO}_2(\text{H}_2\text{O})_3^{1+}$	1	4	1.743	2.456	1.32	-0.39	-0.82	0.49	-933.60248
$\text{PuO}_2(\text{H}_2\text{O})_4^{1+}$	1	4	1.752	2.498	1.27	-0.41	-0.82	0.48	-1010.01966
$\text{PuO}_2(\text{H}_2\text{O})_5^{1+}$	1	4	1.757	2.568	1.17	-0.42	-0.82	0.47	-1086.42230
<i>cis</i> - $\text{PuO}_2(\text{Cl})_2(\text{H}_2\text{O})_2$	0	3	1.72	2.488	0.96	-0.342	-0.79	0.49	-1777.72976
<i>trans</i> - $\text{PuO}_2(\text{Cl})_2(\text{H}_2\text{O})_2$	0	3	1.72	2.464	1.03	-0.34	-0.79	0.48	-1777.73405
<i>cis</i> - $\text{PuO}_2(\text{Cl})_2(\text{H}_2\text{O})_3$	0	3	1.72	2.582	0.97	-0.34	-0.80	0.47	-1854.13428
<i>trans</i> - $\text{PuO}_2(\text{Cl})_2(\text{H}_2\text{O})_3$	0	3	1.72	2.523	1.04	-0.33	-0.79	0.47	-1854.14221
$\text{UO}_2(\text{NO}_3)_2(\text{H}_2\text{O})_2$	0	1	1.755	2.527	1.66	-0.39	-0.81	0.48	-1340.93304
$\text{UO}_2(\text{NO}_3)_2(\text{H}_2\text{O})_3$	0	1	1.755	2.526	1.54	-0.39	-0.82	0.48	-1417.32142

^a PuO_2^{2+} can accommodate only five water molecules in first shell; the sixth water molecule starts forming a second shell (at 4.133 Å) around the PuO_2^{2+} ion.

Table 4. Calculated Bond Distance and Atomic Mulliken Charges of Common Pu(IV) Complexes

complex	q	m	Pu–O _w	Pu–X (X = Cl/O _N)	$q(\text{Pu})$	$q(\text{X})$	$q(\text{O}_w)$	$q(\text{H}_w)$	energy
$\text{Pu}(\text{H}_2\text{O})_8^{4+}$	4	5	2.41		2.09		-0.85	0.54	-1163.68949
$\text{Pu}(\text{NO}_3)_2(\text{H}_2\text{O})_2^{2+}$	2	5	2.394	2.246	1.96	-0.42	-0.85	0.53	-1266.71432
				3.906		-0.17			
$\text{Pu}(\text{NO}_3)_2(\text{H}_2\text{O})_4^{2+}$	2	5	2.420	2.316	1.87	-0.45	-0.84	0.52	-1419.61169
				3.970		-0.23			
$\text{Pu}(\text{NO}_3)_4(\text{H}_2\text{O})_3$	0	5	2.510		1.73	-0.44	-0.82	0.48	-1904.26732
$\text{PuCl}_2(\text{H}_2\text{O})_6^{2+}$	2	5	2.467	2.512	1.18	-0.16	-0.83	0.51	-1932.38799
$\text{PuCl}_4(\text{H}_2\text{O})_4$	0	5	2.545	2.391	1.01	-0.28	-0.82	0.47	-2700.52621
			4.216	2.575		-0.60			

was tested as $-\text{CO}$ group is known to form strong coordination complexes with d-block elements. As shown in Figure 4b, $-\text{CO}$ group attached to the graphene causes rearrangement of nitrates around Pu(IV) ion to accommodate carbonyl group, indicating strong interaction. The MEPs for two cases are shown in Figure 4c,d. A clear picture emerges by observing the change in MO diagrams (Figure 5). The approaching plutonium nitrate complex causes localization of HOMO and

LUMO and thus significantly reduces the current, as will be discussed in later sections.

Molecular Orbital Diagrams. The current–voltage characteristics of the molecular junction can be understood by observing the MOs involved in electron transport. If the MO covers the entire molecule (delocalized), there are high probabilities of electron transport at energies similar to the one of the MO and hence have high conductance. On the contrary, if the MO is localized in a region of the molecule, the

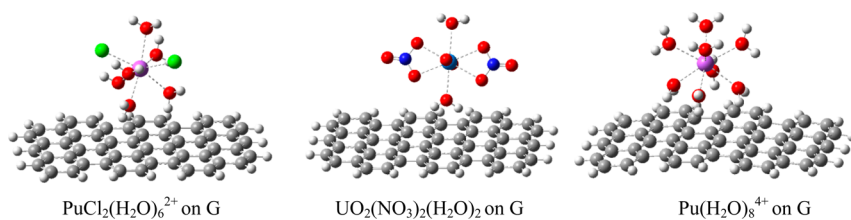


Figure 2. Optimized geometries of some common U and Pu moieties adsorbed on a graphene (G) molecule.

Table 5. Calculated Bond Distances, Atomic Mulliken Charges, and Energies of Pu Complexes Adsorbed on Graphene

complex	Pu–O	Pu–O _w	Pu–X (X = Cl/O _N)	<i>q</i> (Pu)	<i>q</i> (O)	<i>q</i> (X)	<i>q</i> (O _w)	<i>q</i> (H _w)	energy
PuO ₂ (H ₂ O) ₅ ²⁺	1.757	2.564		1.16	-0.42	NA	-0.81	0.48	-3155.46987
cis-PuO ₂ Cl ₂ (H ₂ O) ₂	1.739	2.543	2.632	0.96	-0.38	-0.44	-0.79	0.48	-3847.03326
Pu(H ₂ O) ₈ ⁴⁺		2.513		1.59			-0.86	0.49	-3233.42383
Pu(NO ₃) ₂ (H ₂ O) ₂ ²⁺		2.458	2.358	1.59		-0.48	-0.86	0.49	-3336.23895
			3.999			-0.30			
Pu(NO ₃) ₂ (H ₂ O) ₄ ²⁺		2.512	2.427	1.50		-0.49	-0.84	0.49	-3489.08394
			4.071			-0.33			
Pu(NO ₃) ₄ (H ₂ O) ₃		2.526	2.874	1.65		-0.45	-0.83	0.48	-3973.56671
			3.323						
PuCl ₂ (H ₂ O) ₆ ²⁺		2.551	2.672	0.93		-0.43	-0.83	0.49	-4001.83962

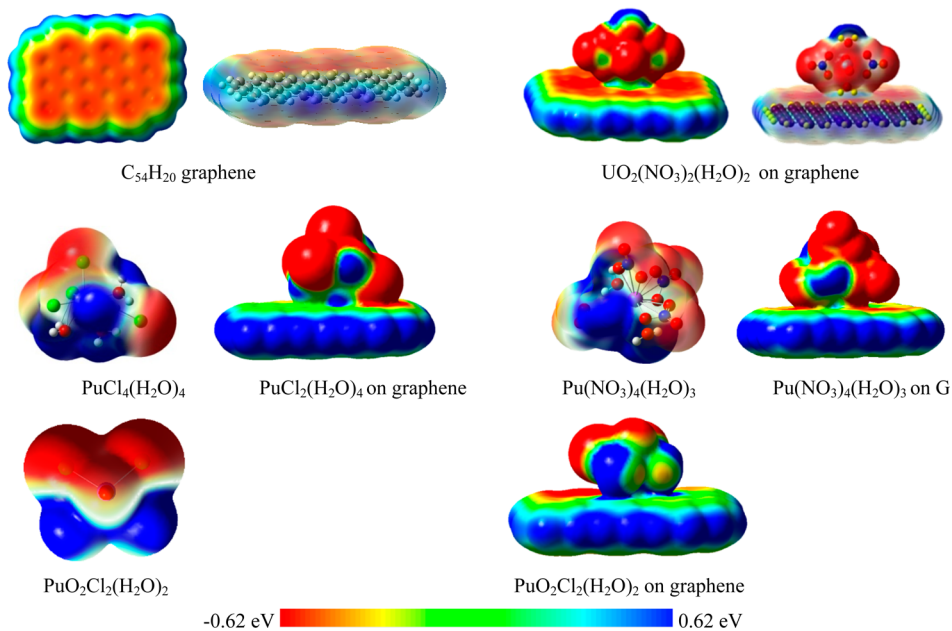


Figure 3. MEPs of U and Pu complexes adsorbed on graphene.

probability of electron transport at energies around the MO energy diminishes, resulting in high impedance. Figure 5a–f shows some of the MOs in the vicinity of highest occupied molecular orbital (HOMO) and lowest unoccupied molecular orbital (LUMO) that are involved in the conduction at low bias voltages for graphene/GO nanosheets used as molecular sensor. The HOMO and LUMO for graphene/GO with Pu(NO₃)₄(H₂O) complex adsorbed on its surface are also presented for comparison.

I–V Characteristics. Green's functions and DFT are used to study electron-transport characteristics through single molecules using two nanometallic contacts. Each contact is modeled using one nanoscopic end (single gold atom) directly bonded to the molecule (graphene-U/Pu complex) and an extended metallic end connected to an external potential

difference. This setting is because the source of electrons is provided by the DOS of the contacts and not by the individual gold atom whose presence is to produce an adequate geometry for the level of theory of the calculation in the neighborhood of the carbon attached to the gold contact. Thus we are assuming in these calculations that the pathway of electrons is through this minimum junction setting. The same setting, for the sake of comparison, is used for all cases that we are analyzing the *I*–*V* characteristics. Certainly, larger sensors would have a larger number of gold atoms attaching to larger size of graphene molecules and yielding larger currents. Although the scalability might not be linear, we understand that the goal is to design the smallest possible sensors; thus, we choose the minimum size point contact for the molecule–electrode interface. The geometries of the molecular junctions Au–molecule–Au

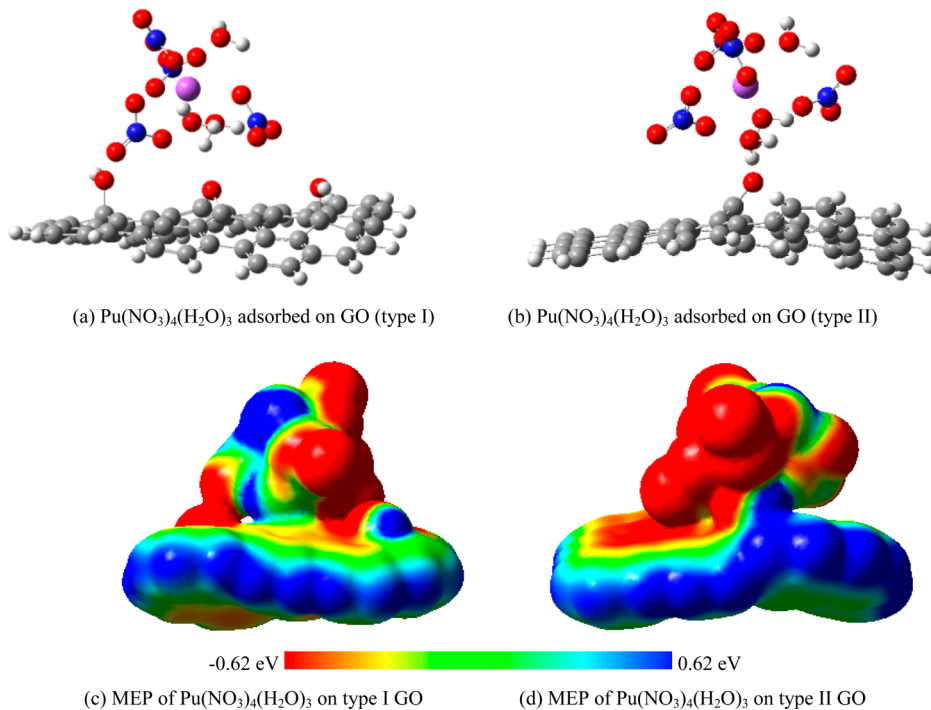


Figure 4. Optimized geometry of nitrato-aquo-complex of Pu(IV) adsorbed on GO (type I) and GO (type II) and their corresponding molecular electrostatic potential (MEP).

(Figure 6) are first fully optimized using the Gaussian program, and their Hamiltonians and overlap matrices are evaluated in the presence of the applied external fields. The DOS of the gold nanocontact is calculated using the Crystal-06 program⁶³ using periodic boundary conditions.

The electron-transport characteristics are then calculated using our in-house GENIP program using a Green's function formalism that requires the Hamiltonian of the molecular junction along with the density of states for the gold nanoelectrodes. The conductance obtained from this approach depends mainly on the energies of the orbitals in the neighborhood of the frontier MOs, the HOMO and the LUMO of the molecular junction as well as on the Fermi level of the electrodes and their coupling to the graphene complex. For small molecules like thioalkanes, results calculated using our GENIP program compare well with experimental values.⁶⁰ It would be difficult to compare current–voltage characteristics of graphene measured experimentally to the results obtained using ab initio calculations due to the fact that we consider only a very small piece of graphene sheet compared with large graphene sheets used for experiments. The minimum sheet resistance for graphene is reported as $6.45 \text{ k}\Omega/\text{sq}$.⁶⁴ On the basis of lateral dimensions and calculated current–voltage characteristics, the sheet resistance is found to be $\sim 1150 \text{ k}\Omega/\text{sq}$, which is consistent with the fact that resistance increases with decrease in number of channels for electron transport, and we consider a single point of contact; thus comparing to experiment, a 200 points-contact or $\sim 60 \text{ nm}$ electrode would yield the same resistance sheet. We find similar trend as reported in literature for electrical conductivities comparing graphene and GO.⁶⁵

The resulting current–voltage characteristics for interaction of plutonium complexes with graphene and GO are shown in Figure 7a. No appreciable change in I – V characteristics of graphene is observed when plutonium complex approaches a

graphene sheet. This can be explained by careful observation of MO pictures for graphene–plutonium complex (Figure 5a,b). There is no appreciable change in π - π orbitals on graphene surface in the presence of Pu^{4+} complex, indicating a weak interaction with graphene and a strong interaction with surrounding nitrate ions. The conductance is found to increase marginally from 0.67 to $0.93 \mu\text{A}\text{V}^{-1}$. Similar results are obtained for GO with $-\text{O}-$ functional group (Figure 5c,d). However, the conductance of GO is found to decrease in this case from 0.007 to $0.006 \mu\text{A}\text{V}^{-1}$. Hence a GO with a carbonyl group is tested for its interaction with plutonium complexes. Introduction of $-\text{CO}$ group on graphene induces complex binding of Pu^{4+} complex, which can be observed by looking at the MO diagrams (Figure 5e,f). As a result, a significant reduction in current values is observed in the presence of plutonium complex (Figure 7c). The conductance of GO in this case reduces significantly from 9.5 to $1.6 \mu\text{A}\text{V}^{-1}$ in the presence of $\text{Pu}(\text{NO}_3)_4(\text{H}_2\text{O})_3$ complex.

From the above results, we can conclude that GO with $-\text{CO}$ group is the most promising sensing material for detection of U/Pu complexes. The change in current–voltage characteristics can be used as a marked signature to identify radionuclides present in nuclear wastewater.

SUMMARY AND CONCLUSIONS

MEP calculated based on ab initio DFT calculations of U and Pu complexes with graphene reveal that graphene needs to be functionalized to act as an effective sensor for detection of fissile materials. From previous knowledge that GO has high affinity for U and Pu complexes,¹¹ we decided to use two types of GO: (a) GO with two $-\text{OH}$ and one $-\text{O}-$ functional groups present (type I) and (b) GO containing a carbonyl functional group (type II) to study their interactions with plutonium complexes. Changes in the MEP due to the presence of these complexes near graphene or GO can be transduced

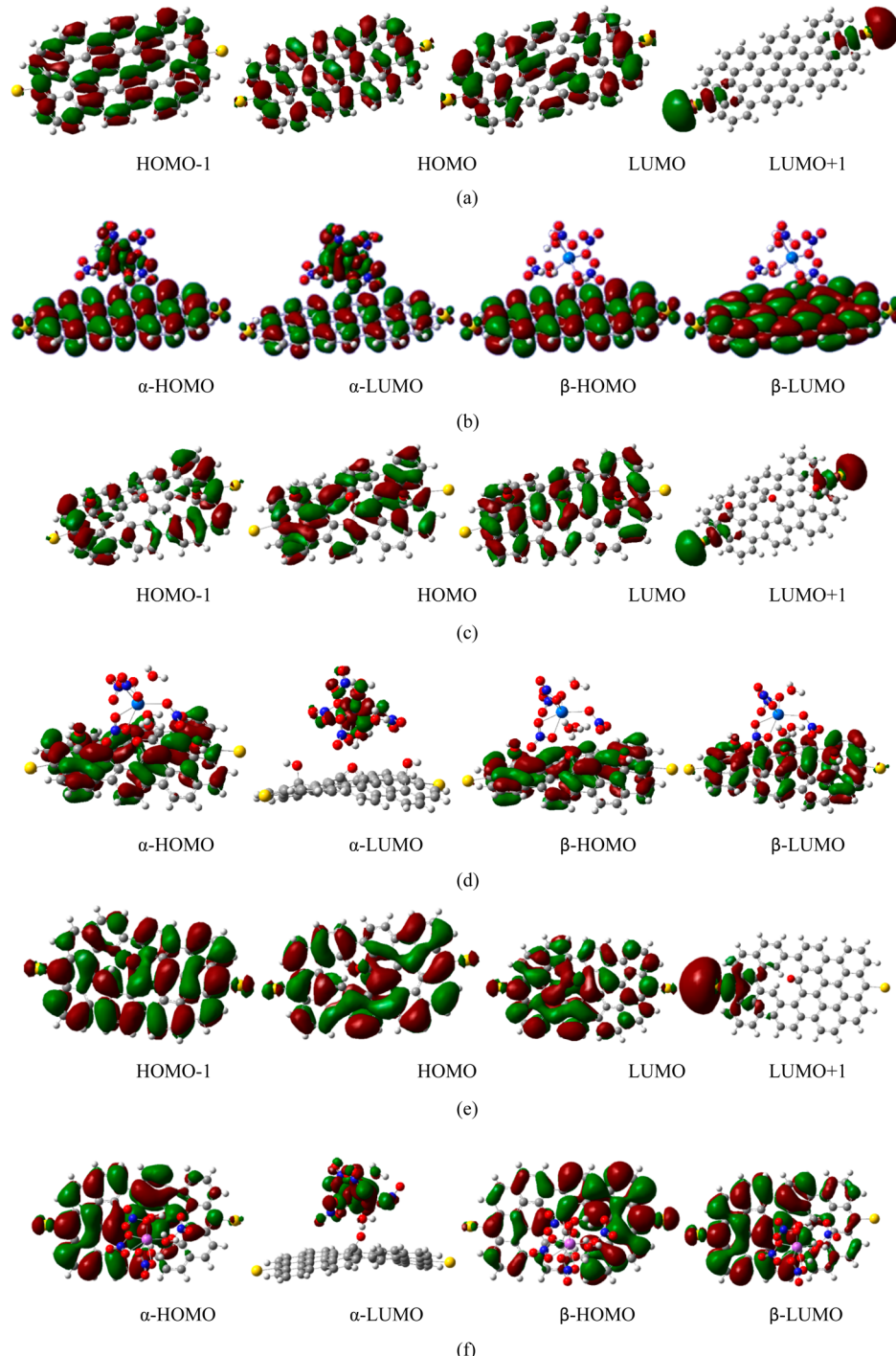


Figure 5. Molecular orbital diagrams of (a) graphene nanosheet, (b) $\text{Pu}(\text{NO}_3)_4(\text{H}_2\text{O})_3$ adsorbed on graphene, (c) graphene oxide GO (type I), (d) $\text{Pu}(\text{NO}_3)_4(\text{H}_2\text{O})_3$ adsorbed on GO (type I), (e) graphene oxide GO (type II), and (f) $\text{Pu}(\text{NO}_3)_4(\text{H}_2\text{O})_3$ adsorbed on GO (type II).

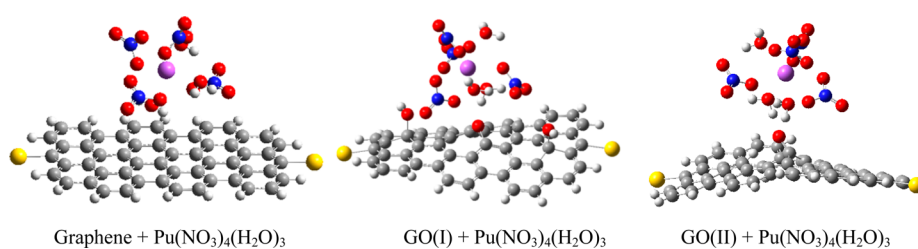


Figure 6. Au–molecule–Au junctions used for generation of I – V characteristics.

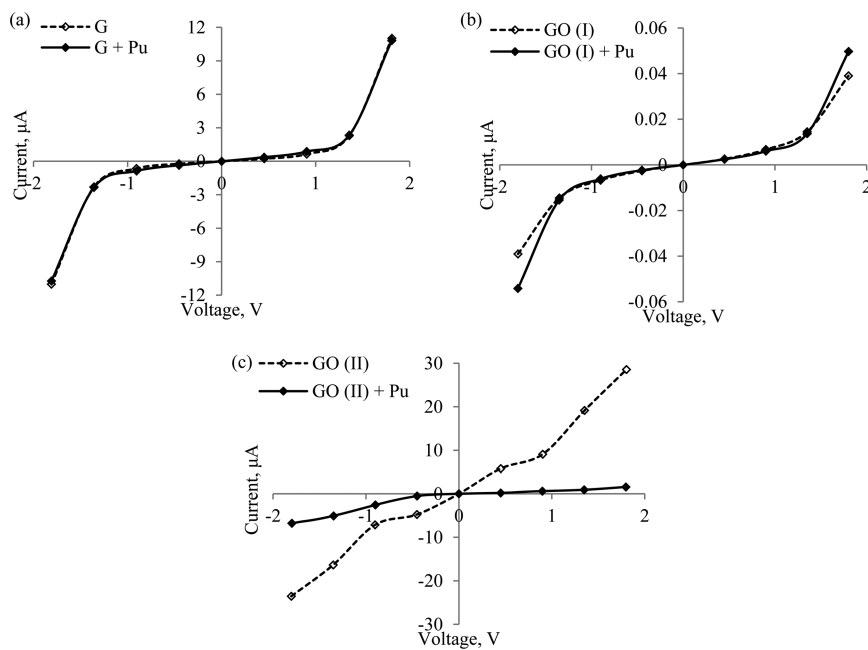


Figure 7. Current–voltage characteristics of Pu(IV) complex adsorbed on graphene/graphene oxide. (a) $(\text{NO}_3)_4(\text{H}_2\text{O})_3$ on graphene. (b) $\text{Pu}(\text{NO}_3)_4(\text{H}_2\text{O})_3$ on GO (type I). (c) $\text{Pu}(\text{NO}_3)_4(\text{H}_2\text{O})_3$ on GO (type II).

and amplified into current–voltage characteristics on the nanoscale. By comparing the changes in current, we should be able to detect trace amounts of these radionuclides.

The current–voltage curves for the graphene/GO along with other moieties are calculated using our in-house program GENIP. Our calculations show significant reduction in current values for given bias voltage when plutonium complexes approach GOs containing –CO functional group as compared with a graphene sheet or type-I GO with –O– functional group due to weak interaction. –CO group attached to graphene surface causes nitrates around central Pu(IV) ion to displace, indicating strong interaction. In addition, approaching plutonium nitrate complex causes localization of HOMO and LUMO, which results in significant reduction in current values.

AUTHOR INFORMATION

Corresponding Author

*Tel: (979)845-3301. Fax: (979)845-3301. E-mail: seminario@tamu.edu.

Notes

The authors declare no competing financial interest.

ACKNOWLEDGMENTS

We acknowledge the high-performance computing support provided by the Texas A&M Supercomputer Facility and the Texas Advanced Computing Center as well as Michael Kaminski and Giselle Sandi-Tapia from the Argonne National Laboratory's Nuclear Forensics and Nanoscale Engineering Group for discussions on the experimental aspects of radioactive nuclides. We also acknowledge the Argonne National Laboratory's Laboratory-Directed Research and Development Strategic Initiative; the U.S. Defense Threat Reduction Agency (DTRA) through the U.S. Army Research Office (ARO), project W91NF-06-1-0231; and ARO/MURI project W911NF-11-1-0024 for their support.

REFERENCES

- Greathouse, J. A.; O'Brien, R. J.; Bemis, G.; Pabalan, R. T. *J. Phys. Chem. B* **2002**, *106*, 1646–1655.
- Craw, J. S.; Vincent, M. A.; Hillier, I. H.; Wallwork, A. L. *J. Phys. Chem.* **1995**, *99*, 10181–10185.
- Blaudeau, J.-P.; Zygmunt, S. A.; Curtiss, L. A.; Reed, D. T.; Bursten, B. E. *Chem. Phys. Lett.* **1999**, *310*, 347–354.
- Choppin, G. R.; Morgenstern, A. Distribution and Movement of Environmental Plutonium. In *Radioactivity in the Environment*; Elsevier: Boston, 2001; Vol. 1, pp 91–105.
- Guilbaud, P.; Wipff, G. *J. Phys. Chem.* **1993**, *97*, 5685–5692.
- Guilbaud, P.; Wipff, G. *J. Mol. Recogn. Inclus. Phenom.* **1993**, *16*, 169–188.
- Guilbaud, P.; W., G. *J. Mol. Struct.: THEOCHEM* **1996**, *366*, 55–63.
- Xianggui, Y.; Smith, R. B.; Shengting, C.; De Almeida, V.; Khomami, B. *Solvent Extr. Ion Exch.* **2010**, *28*, 1–18.
- Duvail, M.; Martelli, F.; Vitorge, P.; Spezia, R. *J. Chem. Phys.* **2011**, *135*, 044503–044510.
- Marjolin, A.; Gourlaouen, C.; Clavaguéra, C.; Ren, P.; Wu, J.; Gresh, N.; Dognon, J.-P.; Piquemal, J.-P. *Theor. Chem. Acc.* **2012**, *131*, 1–14.
- Romanchuk, A. Y.; Slesarev, A. S.; Kalmykov, S. N.; Kosynkin, D. V.; Tour, J. M. *Phys. Chem. Chem. Phys.* **2013**, *15*, 2321–2327.
- Rangel, N. L.; Seminario, J. M. *J. Chem. Phys.* **2010**, *132*, 125102 (pages 1–4).
- Sheka, E. F.; Popova, N. A. *Phys. Chem. Chem. Phys.* **2013**, *15*, 13304–13322.
- Lahaye, R. J. W. E.; Jeong, H. K.; Park, C. Y.; Lee, Y. H. *Phys. Rev. B* **2009**, *79*, 125435.
- Hernández Rosas, J. J.; Ramírez Gutiérrez, R. E.; Escobedo-Morales, A.; Chigo Anota, E. *J. Mol. Model.* **2011**, *17*, 1133–1139.
- Dreyer, D. R.; Park, S.; Bielawski, C. W.; Ruoff, R. S. *Chem. Soc. Rev.* **2010**, *39*, 228–240.
- Spencer, S.; Gagliardi, L.; Handy, N. C.; Ioannou, A. G.; Skylaris, C.-K.; Willetts, A.; Simper, A. M. *J. Phys. Chem. A* **1999**, *103*, 1831–1837.
- Majumdar, D.; Balasubramanian, K. *Chem. Phys. Lett.* **2004**, *397*, 26–33.
- Cao, Z.; Balasubramanian, K. *J. Chem. Phys.* **2005**, *123*, 114309.

- (20) Chaudhuri, D.; Balasubramanian, K. *Chem. Phys. Lett.* **2004**, *399*, 67–72.
- (21) Balasubramanian, K.; Chaudhuri, D. *Chem. Phys. Lett.* **2008**, *450*, 196–202.
- (22) Ismail, N.; Heully, J.-L.; Saue, T.; Daudey, J.-P.; Marsden, C. J. *Chem. Phys. Lett.* **1999**, *300*, 296–302.
- (23) Odoh, S. O.; Schreckenbach, G. *J. Phys. Chem. A* **2011**, *115*, 14110–14119.
- (24) Buz'ko, V.; Chuiko, G.; Kushkhov, K. *Russ. J. Inorg. Chem.* **2012**, *57*, 62–67.
- (25) Hohenberg, P.; Kohn, W. *Phys. Rev. B* **1964**, *136*, 864–871.
- (26) Kohn, W.; Sham, L. *J. Phys. Rev. A* **1965**, *140*, 1133–1138.
- (27) Becke, A. D. *J. Chem. Phys.* **1993**, *98*, 5648–5652.
- (28) Roothaan, C. C. *J. Rev. Mod. Phys.* **1951**, *23*, 69–89.
- (29) Pople, J. A.; Nesbet, R. K. *J. Chem. Phys.* **1954**, *22*, 571–572.
- (30) McWeeny, R.; Diercksen, G. *J. Chem. Phys.* **1968**, *49*, 4852–4856.
- (31) Perdew, J. P.; Chevary, J. A.; Vosko, S. H.; Jackson, K. A.; Pederson, M. R.; Singh, D. J.; Fiolhais, C. *Phys. Rev. B* **1993**, *48*, 4978–4978.
- (32) Perdew, J. P.; Chevary, J. A.; Vosko, S. H.; Jackson, K. A.; Pederson, M. R.; Singh, D. J.; Fiolhais, C. *Phys. Rev. B* **1992**, *46*, 6671–6687.
- (33) Perdew, J. P.; Burke, K.; Wang, Y. *Phys. Rev. B* **1996**, *54*, 16533–16539.
- (34) Perdew, J. P. Unified Theory of Exchange and Correlation beyond the Local Density Approximation. In *Electronic Structure of Solids*; Ziesche, P., Eschrig, H., Eds.; Akademie Verlag: Berlin, 1991; pp 11–20.
- (35) Burke, K.; Perdew, J. P.; Wang, Y. In *Electronic Density Functional Theory: Recent Progress and New Directions*; Dobson, J. F., Vignale, G., Das, M. P., Eds.; Plenum Press: New York, 1998.
- (36) Perez-Angel, E. C.; Seminario, J. M. *J. Phys. Chem. C* **2011**, *115*, 6467–6477.
- (37) Cárdenas-Jirón, G. I.; Leon-Plata, P.; Cortes-Arriagada, D.; Seminario, J. M. *J. Phys. Chem. C* **2011**, *115*, 16052–16062.
- (38) Liuming, Y.; Eddy, J. B.; Jorge, M. S. *Nanotechnology* **2007**, *18*, 485701–485701–485708.
- (39) Fu, M.-L.; Rangel, N.; Adams, R.; Seminario, J. J. *Cluster Sci.* **2010**, *21*, 867–878.
- (40) Seminario, J. M.; Araujo, R. A.; Yan, L. *J. Phys. Chem. B* **2004**, *108*, 6915–6918.
- (41) Seminario, J. M.; Derosa, P. A.; Cordova, L. E.; Bozard, B. H. *IEEE Trans. Nanotechnol.* **2004**, *3*, 215–218.
- (42) Balbuena, P. B.; Altomare, D.; Agapito, L. A.; Seminario, J. M. *J. Phys. Chem. B* **2003**, *107*, 13671–13680.
- (43) Derosa, P. A.; Seminario, J. M.; Balbuena, P. B. *J. Phys. Chem. A* **2001**, *105*, 7917–7925.
- (44) Zacarias, A. G.; Castro, M.; Tour, J. M.; Seminario, J. M. *J. Phys. Chem. A* **1999**, *103*, 7692–7700.
- (45) Seminario, J. M.; Zacarias, A. G.; Castro, M. *Int. J. Quantum Chem.* **1997**, *61*, 515–523.
- (46) Seminario, J. M.; Agapito, L. A.; Yan, L.; Balbuena, P. B. *Chem. Phys. Lett.* **2005**, *410*, 275–281.
- (47) Seminario, J. M.; Tour, J. M. *Int. J. Quantum Chem.* **1997**, *65*, 749–758.
- (48) Seminario, J. M.; Ma, Y.; Agapito, L. A.; Yan, L.; Araujo, R. A.; Bingi, S.; Vadlamani, N. S.; Chagarlamudi, K.; Sudarshan, T. S.; Myrick, M. L.; Colavita, P. E.; Franzon, P. D.; Nackashi, D. P.; Cheng, L.; Yao, Y.; Tour, J. M. *J. Nanosci. Nanotechnol.* **2004**, *4*, 907–917.
- (49) Frisch, M. J.; Trucks, G. W.; Schlegel, H. B.; Scuseria, G. E.; Robb, M. A.; Cheeseman, J. R.; Scalmani, G.; Barone, V.; Mennucci, B.; Petersson, G. A.; Nakatsuji, H.; Caricato, M.; Li, X.; Hratchian, H. P.; Izmaylov, A. F.; Bloino, J.; Zheng, G.; Sonnenberg, J. L.; Hada, M.; Ehara, M.; Toyota, K.; Fukuda, R.; Hasegawa, J.; Ishida, M.; Nakajima, T.; Honda, Y.; Kitao, O.; Nakai, H.; Vreven, T.; Montgomery, J. A., Jr.; Peralta, J. E.; Ogliaro, F.; Bearpark, M.; Heyd, J. J.; Brothers, E.; Kudin, K. N.; Staroverov, V. N.; Kobayashi, R.; Normand, J.; Raghavachari, K.; Rendell, A.; Burant, J. C.; Iyengar, S. S.; Tomasi, J.; Cossi, M.; Rega, N.; Millam, N. J.; Klene, M.; Knox, J. E.; Cross, J. B.; Bakken, V.; Adamo, C.; Jaramillo, J.; Gomperts, R.; Stratmann, R. E.; Yazyev, O.; Austin, A. J.; Cammi, R.; Pomelli, C.; Ochterski, J. W.; Martin, R. L.; Morokuma, K.; Zakrzewski, V. G.; Voth, G. A.; Salvador, P.; Dannenberg, J. J.; Dapprich, S.; Daniels, A. D.; Farkas, Ö.; Foresman, J. B.; Ortiz, J. V.; Cioslowski, J.; Fox, D. J. *Gaussian 09*, revision B.01; Gaussian, Inc.: Wallingford, CT, 2009.
- (50) Cao, X.; Dolg, M.; Stoll, H. *J. Chem. Phys.* **2003**, *118*, 487.
- (51) Cao, X.; Dolg, M. *J. Mol. Struct.: THEOCHEM* **2004**, *673*, 203–209.
- (52) Hay, P. J.; Wadt, W. R. *J. Chem. Phys.* **1985**, *82*, 270–283.
- (53) Hay, P. J.; Wadt, W. R. *J. Chem. Phys.* **1985**, *82*, 299–310.
- (54) Wadt, W. R.; Hay, P. J. *J. Chem. Phys.* **1985**, *82*, 284–298.
- (55) Hehre, W. J.; Ditchfield, R.; Pople, J. A. *J. Chem. Phys.* **1972**, *56*, 2257.
- (56) Peng, C.; Ayala, P. Y.; Schlegel, H. B.; Frisch, M. J. *J. Comput. Chem.* **1996**, *17*, 49–56.
- (57) Li, X.; Frisch, M. J. *J. Chem. Theory Comput.* **2006**, *2*, 835–839.
- (58) Derosa, P. A.; Seminario, J. M. *J. Phys. Chem. B* **2000**, *105*, 471–481.
- (59) Seminario, J. M.; Zacarias, A. G.; Derosa, P. A. *J. Chem. Phys.* **2002**, *116*, 1671–1683.
- (60) Seminario, J. M.; Yan, L. *Int. J. Quantum Chem.* **2005**, *102*, 711–723.
- (61) Rios, D.; Michelini, M. C.; Lucena, A. F.; Marçalo, J.; Bray, T. H.; Gibson, J. K. *Inorg. Chem.* **2012**, *51*, 6603–6614.
- (62) Blaise, J.; Wyart, J. F. *Energy Levels and Atomic Spectra of Actinides, International Tables of Selected Constants* 1992; Vol. 20.
- (63) Dovesi, R.; Saunders, V. R.; Roetti, C.; Orlando, R.; Zicovich-Wilson, C. M.; Pascale, F.; Civalleri, B.; Doll, K.; Harrison, N. M.; Bush, I. J.; D'Arco, P.; Llunell, M. *CRYSTAL06 User's Manual*; University of Torino: Torino, 2006.
- (64) Geim, A. K.; Novoselov, K. S. *Nat. Mater.* **2007**, *6*, 183–191.
- (65) Punckt, C.; Muckel, F.; Wolff, S.; Aksay, I. A.; Chavarin, C. A.; Bacher, G.; Mertin, W. *Appl. Phys. Lett.* **2013**, *102*, 023114–023115.